Effect of Carbide Dissolution on Chlorine Induced High Temperature Corrosion of HVOF and HVAF Sprayed Cr3C2-NiCrMoNb Coatings

D. Fantozzi[a], V. Matikainen[a], M. Uusitalo[b], H. Koivuluoto[a], P.Vuoristo[a]
[a] Tampere University of Technology, Laboratory of Materials Science, Tampere / FIN
[b] Valmet Technologies Ltd., Tampere / FIN

This is a post-peer-review, pre-copyedit version of an article published in Journal of Thermal spray Technology.
The final authenticated version is available online at: *https://doi.org/10.1007/s11666-017-0645-3*.

Abstract

Highly corrosion and wear resistant thermally sprayed chromium carbide (Cr_3C_2) based cermet coatings are nowadays a potential highly durable solution to allow traditional fluidised bed combustors (FBC) to be operated with ecological waste and biomass fuels. However, the heat input of thermal spray causes carbide dissolution in the metal binder. This results in the formation of carbon saturated metastable phases, which can affect the behaviour of the materials during exposure. This study analyses the effect of carbide dissolution in the metal matrix of Cr_3C_2-50NiCrMoNb coatings and its effect on chlorine induced high temperature corrosion. Four coatings were thermally sprayed with HVAF and HVOF techniques in order to obtain microstructures with increasing amount of carbide dissolution in the metal matrix. The coatings were heat-treated in an inert argon atmosphere to induce secondary carbide precipitation. As-sprayed and heat-treated self-standing coatings were covered with KCl and their corrosion resistance was investigated with thermogravimetric analysis (TGA) and ordinary high temperature corrosion test at 550˚C for 4 hours and 72 hours, respectively. High carbon dissolution in the metal matrix appeared to be detrimental against chlorine induced high temperature corrosion. The microstructural changes induced by the heat treatment hindered the corrosion onset in the coatings.

Keywords: HVOF, HVAF, chlorine induced high temperature corrosion, carbide dissolution

1 Introduction

Fossil combustion-based energy production needs to be replaced by renewable sources in order to reduce greenhouse gas emissions. Biomass and municipal solid waste (MSW) are ecological alternatives to fossil fuels able to lead the industry of power generation to a greener new era. It has been estimated that replacing only 10% of the coal combusted worldwide with biomass would reduce the annual emissions by 450 M tonnes of CO_2 (Ref 1). However, such fuels have high content of corrosive

agents that cause a severe accelerated corrosion mechanism known as chlorine active oxidation (Ref 2-5). Erosion phenomena are also often present, especially in fluidised bed combustors (FBC), and they further increase materials losses. These problems are enhanced by temperature and therefore, to minimise materials degradation, boilers burning waste and biomass must be operated at lower steam temperatures than traditional coal fired boilers. Unfortunately, this results in a drastic loss of energy efficiency and overall performance (Ref 6-8). Currently, there are no materials able to offer adequate erosion-corrosion protection in the most severe environments. The gap between the industrial need and the available materials causes significant efficiency performance losses in power plants. Therefore, novel highly erosion-corrosion resistant protective materials or coatings are required. Thermal spraying is one of the most versatile surface engineering techniques to produce thick (20-1000 μm) coatings. Metallic alloys such as NiCrMoNb, often designated as alloy 625, are widely applied to protect waste-to-energy (WtE) (Ref 9-11) and biomass (Ref 12, 13) boiler tubes in extreme purely corrosive environments. However, high flue gas and ash particle velocities, soot blowing and fluidised bed media generates harsh erosive conditions which pure metallic materials are not able to withstand (Ref 14). The state-of-the-art materials in erosion-corrosion applications are metal matrix composite (MMC) coatings with Cr_3C_2-NiCr being the most common composition for high temperature wear applications (Ref 15). In such compositions, the hard carbides bear the erosive load while the alloy binder bears the corrosive load. However, in the presence of chlorine, the corrosive load is very high and novel material compositions are required. In this study, a modern Cr_3C_2-NiCrMoNb coating composition was studied. The superalloy matrix (alloy 625) is designed to provide higher corrosion protection than the traditional NiCr alloy (Ref 16).). NiCrMoNb alloys are thought to offer augmented corrosion resistance compared to the traditional NiCr and NiCrBSi alloys in oxidizing-chloridizing environment. The improvements are attributed to the beneficial role of Mo and Nb, which are widely confirmed in literature (Ref 17-20). Indeed, the formation of a protective oxide film of MoO_2 and Nb_2O_5 the vicinity of the scale–alloy interface was proved to suppress the corrosion rate (Ref 21). However, extremely limited information is available in literature about the thermally sprayed coatings deposited with such composition (Ref 16, 22, 23) and further knowledge is therefore needed.

Unfortunately, MMC materials experience severe degradation in boilers because of the high reactivity of carbides in presence of chlorine (Ref 14, 24). During thermal spraying, a combustion process heats and softens the powder particles of the feedstock material, which are then accelerated towards the substrate where upon impact, flatten and by rapid solidification build the coating (Ref 25). Due to the heat input of the process, a portion of the carbides in the feedstock material are melted and diluted into the metal matrix. Rapid solidification of the particles results in the formation of a metastable C- and Cr-rich alloy (Ref 26, 27). Under exposure to high temperature, enough energy is available to enable the metastable matrix to undergo various microstructural refinements including the precipitation of fine secondary carbide phases and thus, achieving a more stable state (Ref 28).

Secondary carbide precipitates and metastable metal matrix composition, being microstructural features, must have an impact on the performance of the coatings. Based on this hypothesis, this work aims to verify whether the secondary carbide precipitates and the metastable composition of the matrix have detrimental effect on the high temperature corrosion resistance of thermally sprayed Cr_3C_2-based coatings in chlorine containing environment. In this study, four Cr_3C_2-NiCrMoNb coatings were sprayed with different melting degrees by varying the spray process and spray parameters. The coatings were prepared with high-velocity air-fuel (HVAF) and high-velocity oxygen-fuel (HVOF) spray processes. HVAF process was used to reach the coldest spray parameters whereas HVOF was used to obtain the hottest ones. The hypothesis is that hotter spray parameters will result in higher carbon dissolution from the carbide hard phase to the matrix. Based on this hypothesis, a heat treatment was carried out on the as-sprayed coatings to induce the precipitation of the dissolved carbon in the metal binder, thus resulting in four coatings with increasing amount of secondary carbide precipitates. The corrosion properties of the as-sprayed and heat-treated coatings were studied with thermogravimetric analyses (TGA) and traditional isothermal corrosion tests.

2 Experimental

2.1 Coating manufacturing

Four coatings of the same composition were deposited with HVOF and HVAF processes from agglomerated and sintered powders (H.C. Starck GmbH, Germany). The Coulter size measurement plots of the particles size distribution is presented in Fig. 1 for the two spray powders. The depositions of the coatings were carried out with M3 HVAF gun (Uniquecoat Technologies LLC, USA) and with Diamond Jet 2700 HVOF gun (Oerlikon Metco, Switzerland). The coating composition was Cr_3C_2-50NiCrMoNb in which the hard phase Cr_3C_2 is dispersed in a NiCrMoNb metal matrix. The coatings were sprayed with two powders with same composition but different particle size distribution. The in-flight particle parameters measured with Spraywatch 4S thermal spray sensor (Oseir Ltd., Finland) and details of the feedstock powders are listed in Table 1. The coarser particle size was exploited to achieve coatings with lower melting degree compared to the fine particle size. The process parameters for the deposition of the coatings are reported in Table 2. The nominal alloy composition of Inconel 625 is 20-23 % Cr, 8-10 % Mo, 3.15-4.15 % Nb, max 5 % Fe and with Ni bal. The process parameters and feedstock powders were chosen in order to obtain four different microstructures with increasing degree of carbon dissolution in the matrix. The coatings were marked as HVAF-grade 1, HVAF-grade 2, HVOF-grade 3 and HVOF-grade 4 with carbon dissolution increasing from grade 1 to grade 4, respectively. However, HVAF-grade 2 and HVOF-grade 3 were sprayed with the most optimised process parameters while the parameters used for the deposition of HVAF-grade 1 and HVOF-grade 4 samples were designed with the main purpose of controlling the amount of melting degree and carbon dissolution in the metal matrix.

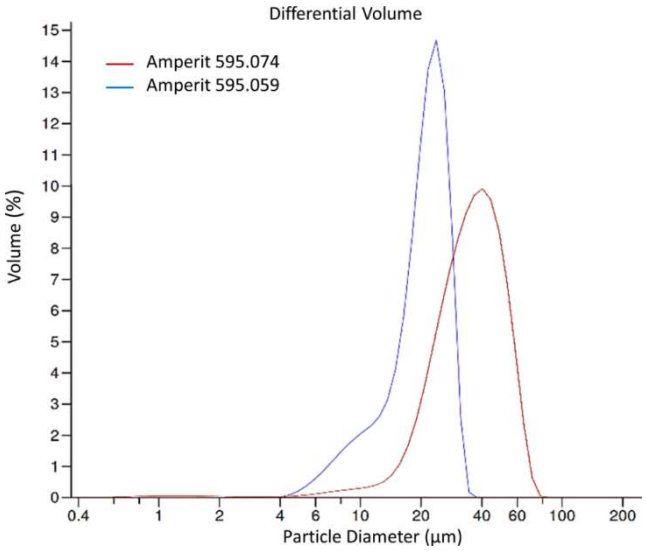

Fig. 1: *Coulter particles size distribution plot of the spray powders.*

Table 1: *Feedstock powder information and in-flight particle properties measured with the SprayWatch 4S thermal spray sensor.*

Code	Powder (H.C. Starck)	Measured mean size [um]	Nominal particle size	Process	Particle Temp. [˚C]	Particle velocity [m/s]
HVAF Grade 1	Amperit 595.074	34.28	-45+15	HVAF M3	1310±3	967±82
HVAF Grade 2	Amperit 595.059	20.23	-30+5	HVAF M3	1460±9	949±109
HVOF Grade 3	Amperit 595.074	34.28	-45+15	HVOF DJ2700	1770±9	767±40
HVOF Grade 4	Amperit 595.059	20.23	-30+5	HVOF DJ2700	1890±5	903±41

Table 2: *Thermal spray process parameters used for HVAF and HVOF coatings*

Parameter	HVAF grade 1	HVAF grade 2	HVOF grade 3 and 4
Nozzle	4L4	4L2	-
Oxygen	-	-	240 slpm
Air	7.4 bar	7.4 bar	383 slpm
Fuel1 (propane)	7.3 bar	7.0 bar	70 slpm
Fuel2 (propane)	6.9 bar	7.3 bar	-
Spray distance	300 mm	300 mm	230 mm

2.2 Sample preparation

The as-sprayed coatings were mechanically removed from the substrate. Prior to the corrosion thermogravimetric tests, the side of the freestanding coating which was originally at the coating-substrate interface was grinded with P1200 SiC abrasive paper in order to remove possible contaminations from the substrate and grit blasting residues. The heat-treated freestanding coatings were grinded on both sides. For the isothermal high temperature corrosion test, all the self-standing coatings were grinded on both sides.

2.3 Heat treatment

The heat treatment was carried out in an in-house built vertical alumina tube furnace under an inert atmosphere (Ar-5 vol.% H_2) at 700˚C for a duration of 5 hours with heating rate of 5 ˚C/min. The samples were cooled down to room temperature in inert atmosphere at a cooling rate of 11 ˚C/min. Similar heat treatment was previously carried out by Ding at al. (Ref 29) on NiCr-Cr_3C_2 coatings, effectively resulting in the precipitation of secondary carbides already after 1 hour of exposure.

2.4 Microstructural characterisation

The microstructures of the coatings were analysed before and after the heat treatment with scanning electron microscope (SEM, Philips XL30, Netherlands) equipped with Energy Dispersive X-ray (EDS) microanalysis. The phase compositions of the as-sprayed and heat-treated coatings were assessed by X-Ray diffractometry (XRD, Empyrean, PANalytical, Netherlands) using Cu-Kα radiation source with 40 mA current and 45 kV voltage.

2.5 Thermogravimetric analyses

The mass changes of the freestanding coatings were measured with thermogravimetric analyser STA 409CD (NETZCH, Germany) equipped with TASC 414/4 temperature controller and PU 1.851.01 power unit to evaluate their corrosion behaviour. In preparation to the measurements, the self-standing coatings were cut to small fragments with an approximate surface of 1 mm^2 each. The total surface area of the samples was measured with image analysis with the software “ImageJ” from optical and stereomicroscope images. The TGA measurements were carried out in alumina crucibles in which the coating fragments were mixed with an excess of potassium chloride powder. The weight of the specimens ranged between 10 and 20 mg while the amount of KCl was about 30 mg. The test atmosphere was dry synthetic air with a gas flow rate of 100 ml/min. The temperature program consisted of a heating ramp of 12 ˚C /min followed by an isothermal step at 550 ˚C for 4 hours. The output data consisted of mass change resulting from the oxidation phenomena that took place during the test plotted in function of time. The absolute mass change was normalised by unit of area [mg/cm^2] in order to compare the samples with each other. The measurements were carried out on three replicas of each coating to assess the repeatability of the test.

2.6 High temperature isothermal test

The isothermal high temperature corrosion test was carried out based on Standard ISO 17224:2015 (E) (Ref 30) in a custom-built horizontal alumina furnace under controlled atmosphere.

The test lasted 72 hours at the temperature of 550˚C. The controlled atmosphere consisted of a constant flow of 1.5l/min of dry air with the addition of water vapour to reach a specific humidity of 10-12%. The self-standing coatings were cut to obtain scales of size of approximately 5x7 mm^2. The coating scales were placed in separate single alumina crucibles containing solid KCl powders. The scales were only partially immersed in the KCl salt, leaving part of the coating not in contact with the salt as schematically represented in Fig. 2.

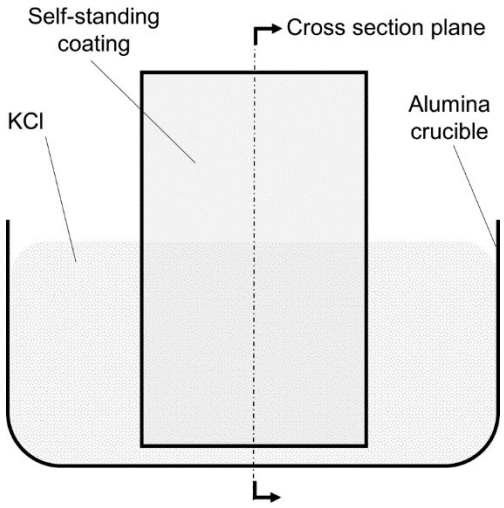

Fig. 2: *Schematic representation of the arrangement of the self-standing coating inside the crucible for the isothermal long-term high temperature corrosion test.*

This set-up allowed the direct visualisation of the degradation of the coating exposed to the salt and its comparison with the unexposed part. Following the test, the coatings were cold mounted in epoxy resin for metallographic inspection. Attention was paid to mount the self-standing coatings in order to expose the interface at the salt level (see cross section plane in Fig. 2). The buttons were then grinded with P500, P1200 and P2000 SiC abrasive papers and polished with subsequent diamond spray clothes down to 0.25 µm. The procedure of sample preparation after the corrosion test was carried out using only ethanol as lubricant and therefore was completely water free in order to prevent the loss of water-soluble

corrosion products. The extent of the corrosion degradation was quantified by measuring the thickness loss of the coatings by image analysis from the SEM images of the cross section. The images were processed with the software "ImageJ" to obtain black and white thresholding of pictures where the coating layer is composed of white pixels. The thickness of each column of white pixel represents the local thickness of the self-standing coating. A "MatLab" script measured the height of each pixel column of unaltered coating and those of the corroded one, then, it calculated the median of their difference. A similar procedure was adopted in our previous work, as well (Ref 31).

3 Results and discussion

The high temperature corrosion behaviour of the heat-treated and as-sprayed coatings is discussed in the following chapters in relation to their microstructural properties.

3.1 Microstructure of coatings

The microstructures of the coating cross-sections were analysed with SEM and reported in Fig. 3. All the sprayed coatings presented highly dense microstructures. The nominal melting point of the metal binder ranges between 1290 and 1350˚C (Ref 32) while the melting point of pure Cr_3C_2 is 1829 ˚C. Therefore, complete melting of the matrix is very likely for the HVOF grade 3 and grade 4 coatings whose measured average particle temperatures at spray distance were 1770 and 1900 ˚C, respectively. In addition, direct melting of the carbide particles is possible in the deposition of HVOF grade 4 coating. For the HVAF coatings, lower particle temperatures were measured (see Table 1) and most probably, only partial melting of the particles took place. Consistent with the design of process parameters, the four coatings showed an increasing amount of melting degree with negligible content in HVAF-grade 1 to significant matrix melting in HVOF-grade 4. Significant melting degree of HVOF carbide based coatings was observed in other studies with typical thin and wide splats (Ref 27, 33, 34), which resemble what observed in the present study. HVAF carbide based coatings resulted in a more homogeneous microstructure with defined carbide particles, similar to those described by other authors in literature (Ref 16, 33, 35).

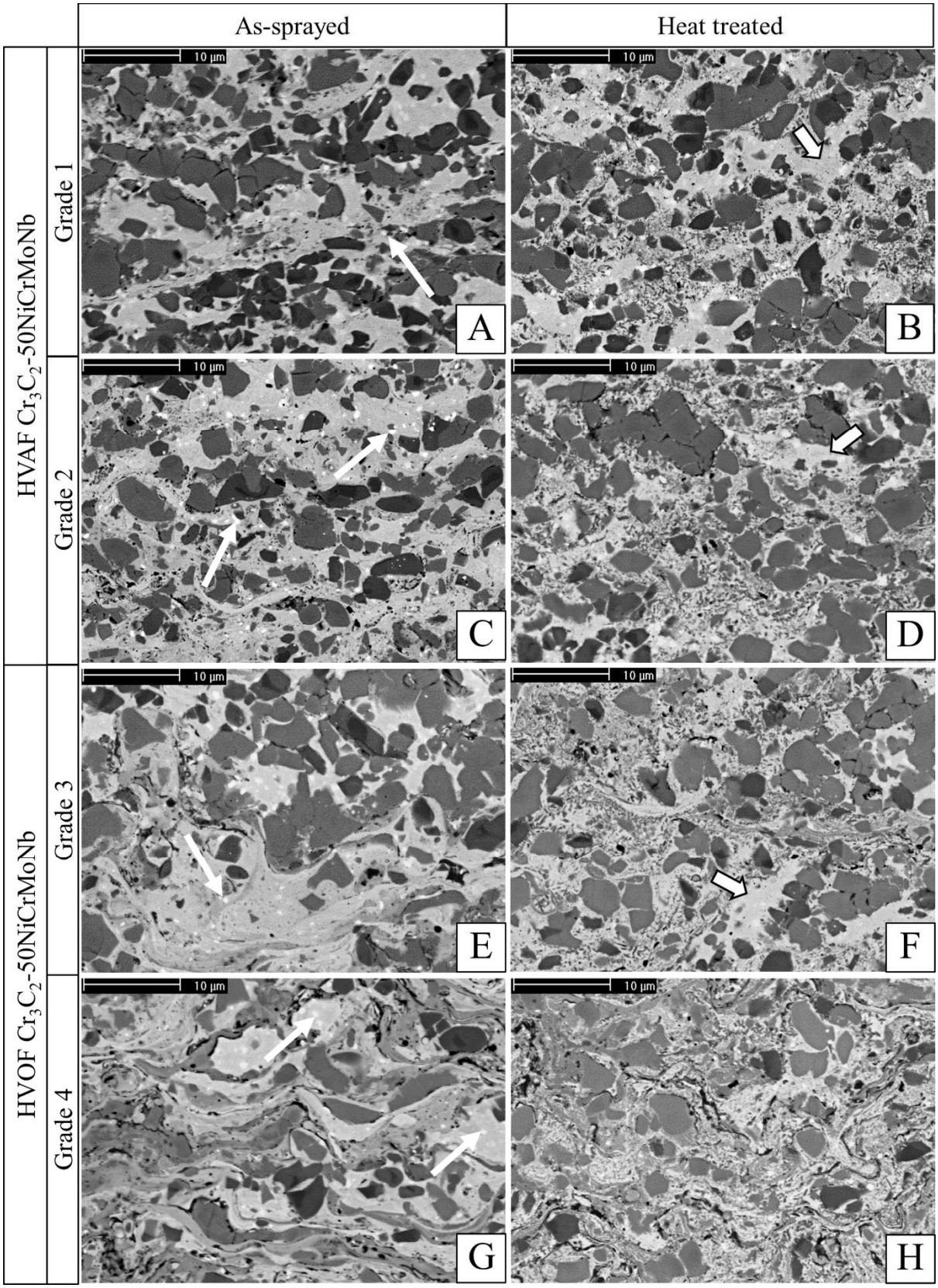

Fig. 3: *SEM (BSE) images of the cross sections of the as-sprayed (HVAF grade 1 (a), HVAF grade 2 (c), HVOF grade 3 (e), HVOF grade 4 and EDS analysis of a NbC particle (g)) and heat-treated coatings HVAF grade 1 (b), HVAF grade 2 (d), HVOF grade 3 (f), HVOF grade 4 (h)). The thick arrows point at areas where no precipitation took place. Thin arrows point at NbC particles.*

All the coatings showed mainly two types of carbides in the SEM images taken with BSE detector. The light coloured ones have higher content of Ni and lower content of Cr than the dark coloured ones. Their composition is perhaps similar to the mixed carbides $(Cr,Ni)_7C_3$ as described by other authors in the past (Ref 36, 37). The amount of Ni enriched carbides seems to be higher in the HVAF-grade 2 and HVOF-grade 4 coatings. The difference is shown also by the XRD patterns in Fig. 4b where the Cr_7C_3 peak intensities (at 38.93°) of grades 2 and 4 are increased in relation to the partially overlapping Cr_3C_2 peak (at 38.77°) compared to the XRD patterns of grades 1 and 3. This indicates that more light grey coloured $(Cr,Ni)_7C_3$ carbides are indeed present in the coatings sprayed from the finer particle size distribution. The fine white coloured dots observed in all the coatings are Nb-rich carbides. In HVOF-grade 3 and 4 coatings, the portion of matrix that was melted during the spraying is clearly visible and presents different grey shades in BSE contrast images deriving from the different levels of carbon dilution.

After heat treatment, fine-grained secondary carbide particles precipitated in the metal binder. Their amount in the coating was incremental from grade 1 to grade 4 as expected. The precipitation seemed to occur especially in the matrix areas that were melted during the spraying and therefore diluted a high amount of carbon from the primary carbide particles. All coatings, especially HVAF-grade 1, contained some areas with little or no precipitate formation as pointed by the white thick arrows in Fig. 3.

The phase compositions of the coatings were studied with XRD. The superimposition of the XRD pattern of the as-sprayed coatings is presented in Fig. 4.

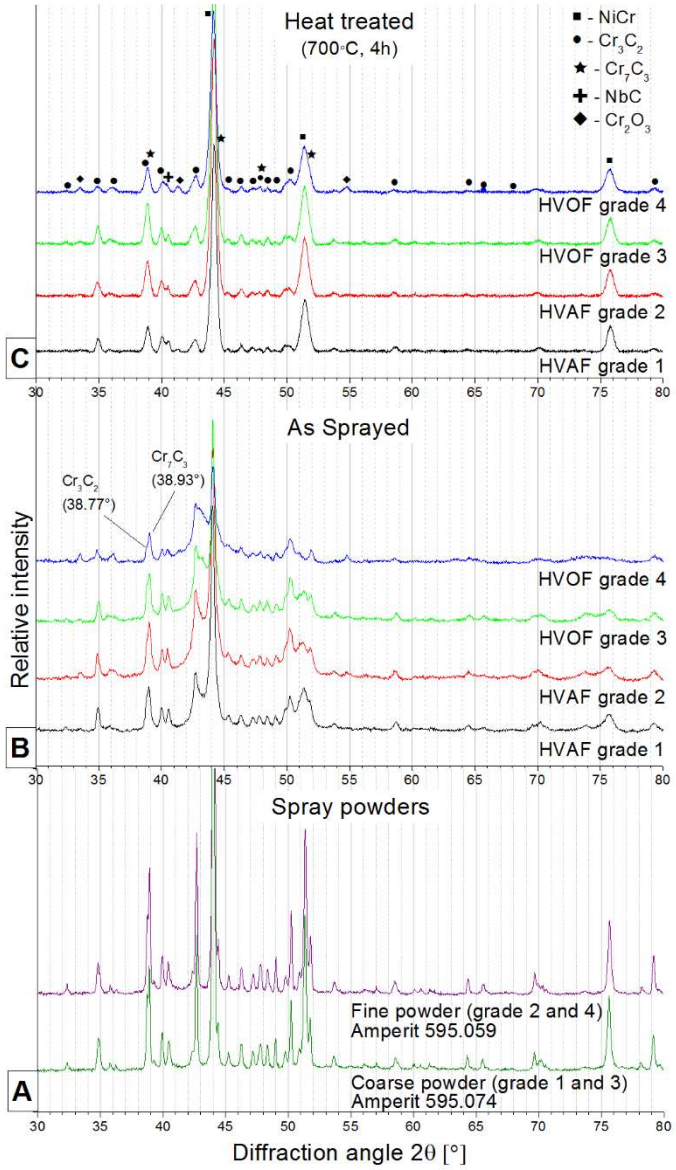

Fig. 4: *Superimposed XRD patterns of: the spray powders (A), as-sprayed coatings (B) and heat-treated coatings (C).*

All as-sprayed coatings presented the same crystallographic phases. The hard phase is composed of two different chromium carbide compounds, namely Cr_3C_2 and Cr_7C_3. NbC was also detected in all the coatings even though in little amount, as it was also observed by SEM/EDS in Fig. 3.

The relatively low intensity of the peaks of the metallic binder denotes higher amount of amorphous and nanocrystalline phase in the metal binder of the as-sprayed coatings (Ref 26, 29), especially in coating HVOF-grade 4. High content of amorphous phase in coating HVOF-grade 4 was expected because of the higher temperature parameters used in its deposition that induced high carbon dissolution in the metal matrix. The following rapid cooling ultimately resulted in a C saturated partly amorphous

metastable alloy. After heat treatment, all coatings showed marked changes in the microstructure. The main observation was related to the significantly higher intensity and definition of the peaks of the metal matrix. This denotes the transformation of metastable amorphous phases in the alloy into a mostly crystalline phase. The Cr_7C_3 has been reported to transform into Cr_3C_2 during short-term isothermal heat treatments (Ref 36), but it was difficult to confirm to take place in the present study. However, slight decrease in the peak intensity of the Cr_7C_3 phase seemed to take place during heat treatment.

3.2 Corrosion behaviour

3.2.1 Early stage corrosion

The early stage corrosion behaviour of the self-standing coatings was measured with thermogravimetric analyses under KCl salt deposit for as-sprayed and heat-treated coatings. The results are presented as mass gain per surface unit during the four hours isothermal step at 550 ˚C in Fig. 5. It is worth noticing that the measurement on the replica samples resulted in very narrow standard deviation denoting the high reliability of the test method.

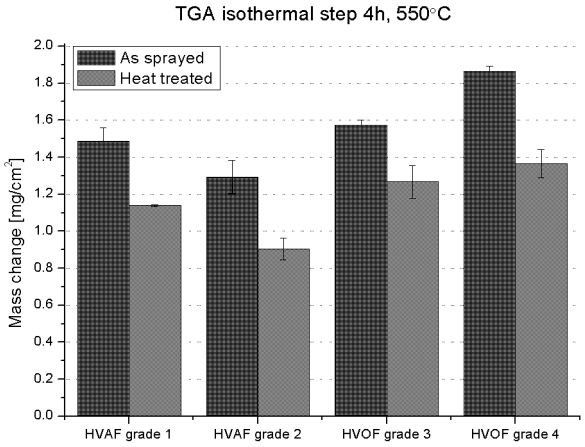

Fig. 5: *Total mass gain of the as-sprayed and heat-treated self-standing coatings during TGA isothermal step at 550 ˚C.*

The results showed some clear trends. Namely, both heat-treated and as-sprayed coatings showed increased corrosion degradation from grade 2 to grade 4, denoting correlation between declined corrosion resistance and warmer spray parameters. The heat-treated samples, despite their higher content of secondary carbide precipitates, always incurred lower mass gain than that of their as-sprayed

counterparts. HVAF-grade 1 represents an exception as it corroded more than HVAF-grade 2 and equally to HVOF-grade 3 which were both deposited with warmer spray parameters. This behaviour, which does not follow the trend of the other coatings, denotes the influence of other variables. HVAF-grade 1 coating present the lowest amount of melting degree and assumingly, the lowest oxide content of all the coatings. These microstructural features are considered helpful in corrosion protection of thermally sprayed coatings. Indeed, they increase sealing among splats and facilitate the formation of appropriate splat morphologies (Ref 31, 35, 38). It is possible that there exists an optimal proportion of oxides content, melting degree and carbon dissolution in the matrix that allow reduced corrosion degradation such as in the case of coating HVAF-grade 2.

The trend observed in the mass gain results of sample HVAF grade 2, HVOF grade 3 and HVOF grade 4 might be explained by the content of carbon dilution in the metal matrix, which increases from grade 2 to grade 4 samples. Therefore, rather than the secondary carbide precipitates, the amount of metastable carbon rich matrix seems to play a role in controlling the corrosion rate at this stage. Indeed, during heat treatment, the excess carbon in the metal matrix is expelled in the form of secondary carbide precipitates (Ref 26). The reduction of C content in the metal binder probably increased its corrosion resistance.

The mass gain in function of time of all the coatings is presented in Fig. 6. The curves can be interpreted as the kinetic of the corrosion mechanism that took place during the TGA.

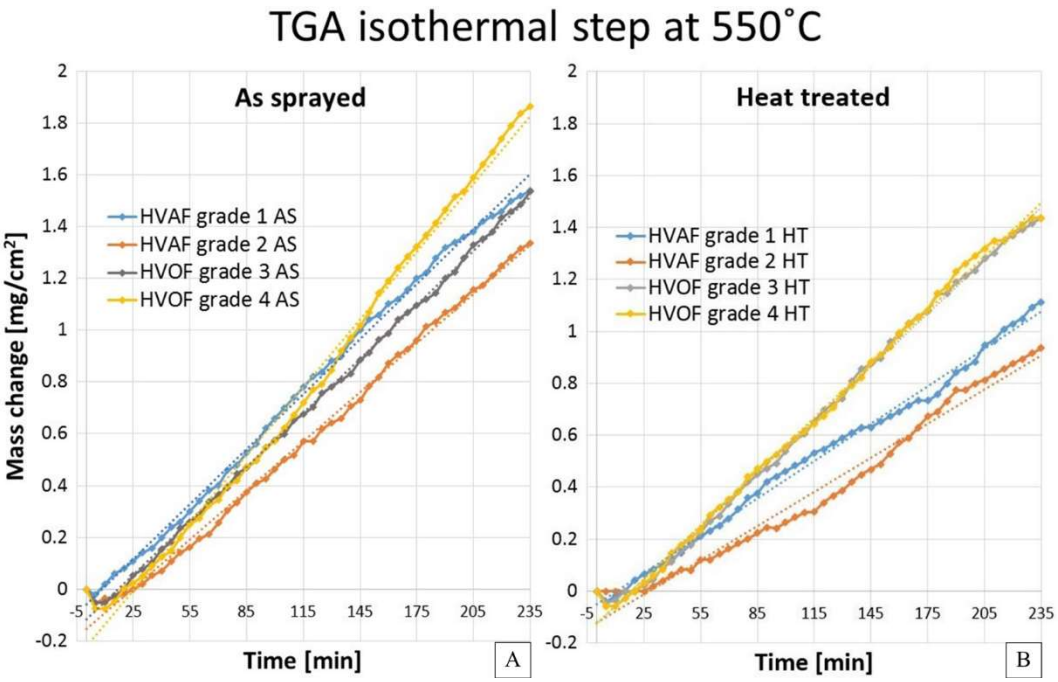

Fig. 6: *TGA mass change curves after four-hour isothermal step at 550˚C of a) the as-sprayed and b) the heat treated samples.*

During the four hours at 550 ˚C, all the samples were subjected to linear corrosion kinetics typical of fast corrosion mechanisms that form porous and non-protective oxide layers (Ref 15, 39). Heat-treated sample HVAF-grade 2, which outperformed all the other coatings, presented the lowest linear constant and a substantial initial delay before starting to gain mass. The chemical reactions that are thought to take place during the test involve the first stages of the chlorine active oxidation mechanism. These include first the reactions between KCl and the oxides embedded in the microstructure and on surface of the coatings as presented in Eq. 1 (Ref 2).

$$Cr_2O_{3\,(s)} + 4KCl_{\,(s)} + \frac{5}{2}O_{2\,(g)} \rightarrow 2K_2CrO_{4\,(s)} + 2Cl_{2\,(g)} \qquad \text{Eq.1}$$

This reaction might also explain the higher corrosion rate of the as-sprayed coatings as the oxides on their surface (deriving from the spray process) might have contributed in the observed mass gain. Secondly, further reactions might have taken place between gaseous Cl_2 evolved from Eq.1 and the metal binder (Eq. 2) or carbides (Eq. 3) based on the following reactions (Ref 40):

$$Cr^{0}_{(s)} + Cl_{2\,(g)} \rightarrow CrCl_{2\,(s)} \qquad \text{Eq. 2}$$

$$Cr_3C_{2\,(s)} + Cl_{2\,(g)} \rightarrow 3CrCl_{2\,(s)} + 2C_{(s)} \qquad \text{Eq. 3}$$

And the subsequent oxidation of the metal chlorides

$$2CrCl_{2\,(g)} + \frac{3}{2}O_{2\,(g)} \rightarrow Cr_2O_{3\,(s)} + 2Cl_{2\,(g)} \qquad \text{Eq. 4}$$

The high airflow rate (100 ml/min) employed in the present tests is thought to provide enough O_2 to complete Eq. 4 and therefore no loss of volatile metal chlorides is supposed. However, in the long term, this assumption might change and therefore, longer thermogravimetric tests will be carried out in the future to further investigate this aspect.

3.2.2 **Prolonged isothermal corrosion resistance**

After the traditional isothermal corrosion test in furnace, the samples were mounted in resin for metallographic inspection with SEM/EDS to evaluate the extent of corrosion degradation. Fig. 7 is a merging of SEM cross sections of the sample HVAF grade 1 HT and serve as illustration of the images used to evaluate the extent of corrosion degradation. This image distinctively show the severe corrosion degradation that KCl induced on the coating. The part of the cross section covered with corrosion products was immersed in the KCl powder as marked in Fig. 7. Although the coating on the left hand side of the cross section was exposed to high temperature and an oxidising environment, it was barely altered due to absence of KCl on its surface.

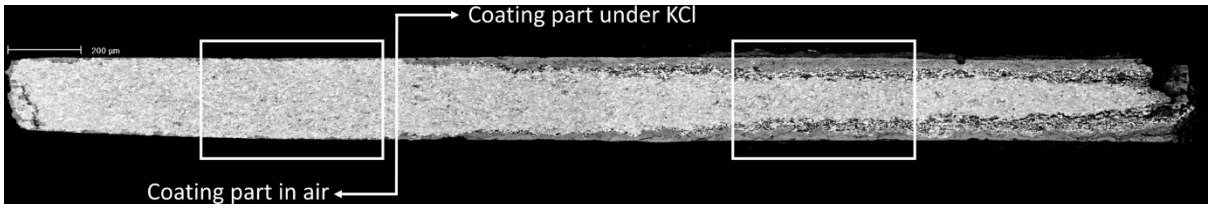

Fig. 7: *Cross section of the corroded sample HVAF-grade 1 HT. The corrosive effect of KCl is clearly visible on the right hand side compared to the not exposed part on the left hand side of the image. The white boxes show the areas where the corresponding thickness was measured.*

The results obtained after traditional high temperature corrosion test in furnace are presented in terms of coating thickness loss in Fig. 8. This data was obtained from the SEM cross section images such as the example reported in Fig. 7, by measuring the difference of coating thickness in the unaltered area and in the corroded one. The unaltered thickness was measured next to the corroded/unaltered interface while the reduced thickness was measured from the centre of the corroded area.

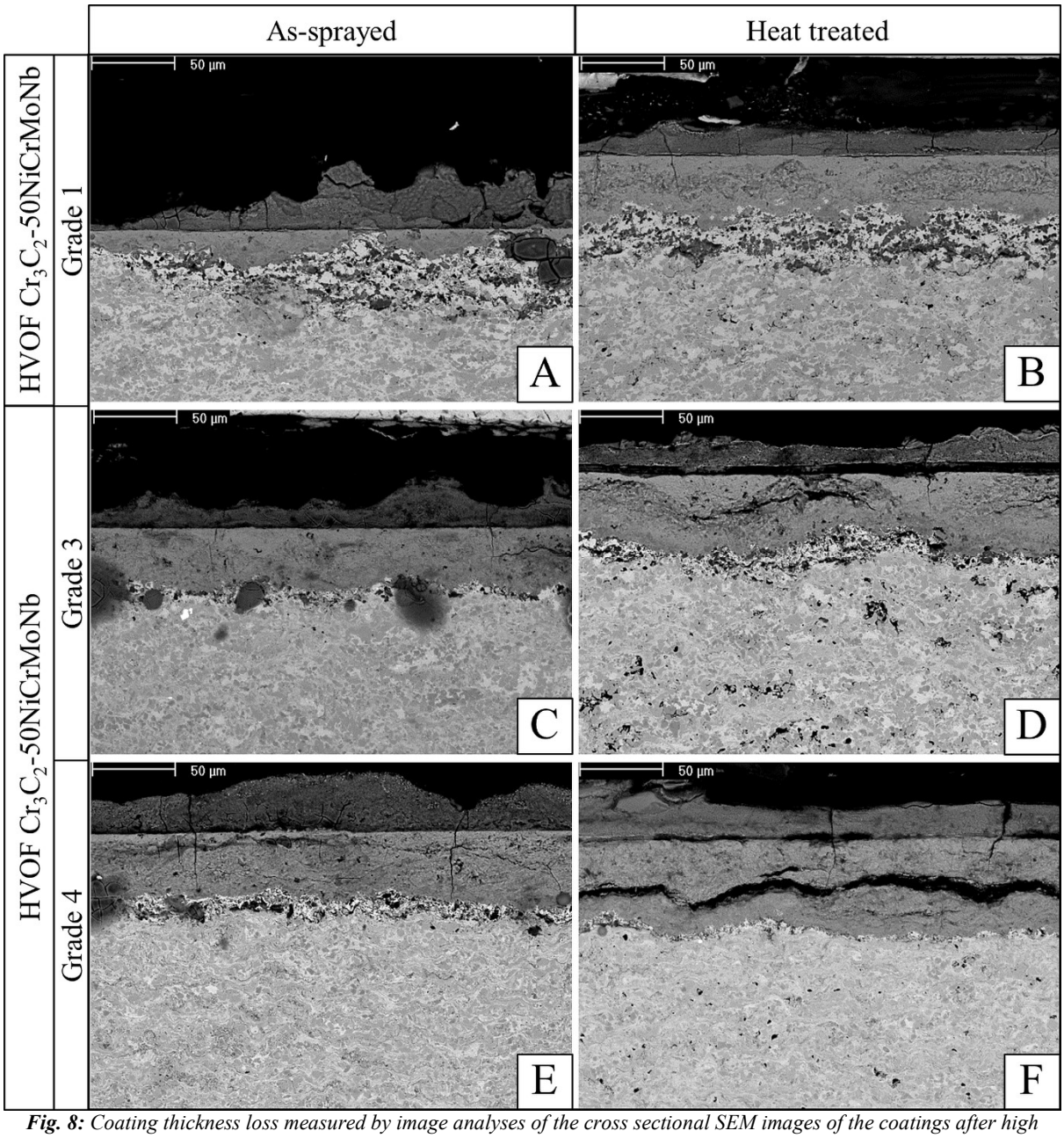

Fig. 8: *Coating thickness loss measured by image analyses of the cross sectional SEM images of the coatings after high temperature corrosion test.*

The observed behaviour is consistent with the results obtained from the thermogravimetric analyses in the short-term exposure test (4h). Indeed, despite the missing data of the as-sprayed HVAF-grade 2 sample, it is clear that the corrosion degradation is more pronounced from grade-2 to grade-4 samples. This finding confirms the hypothesis that carbon dilution and secondary carbide precipitation negatively affects the corrosion resistance of these coatings. However, sample HVAF grade-1 seems to be an exception. The reasons lay probably in other microstructural defects, which may include higher porosity and lower particle deformation at spraying due to the large particle size and low particle temperature (Ref 12, 35, 41). Interestingly, the gap between the as-sprayed coatings and their heat-treated counterparts seems reduced compared to those observed from TGA. In fact, after the 72h test the heat-treated and as-sprayed coatings showed almost equal amount of thickness loss. This would implicate that after a slower corrosion rate in the initial stage, the heat treated coatings underwent higher corrosion rate compared to the not heat treated ones, which resulted in a final reduction of thickness loss gap measured between as-sprayed and the treated samples. This would confirm the hypothesis that initially the composition of the metal matrix is the rate-controlling factor. This results in slower corrosion of the heat-treated samples, which had reduced carbon content due to carbide precipitation. On a later stage, the already present carbides of the heat-treated samples are already enough developed to form an interconnected network. The fine size of the secondary carbide precipitates and their high reactivity with chlorine result in the formation of a wide network of voids as corrosion proceeds. This facilitates further penetration of corrosive agents resulting in an accelerated corrosion with rate controlled by the secondary carbide precipitates. On the other hand, in the as-sprayed coatings, the matrix-controlled stage is faster but then, the network of secondary carbides it not fully developed yet and the second stage is delayed. The fast degradation of the secondary carbide precipitates negatively affects also the resistance of the surrounding metal matrix since the voids creating a larger active area to which the matrix is exposed. Fig. 9 presents the SEM cross section images of the coatings after the high temperature corrosion test and show how the fast degradation of the secondary carbides is detrimental also the resistance of the matrix itself. For instance, in Fig. 9e, the corrosion front of the as-sprayed coating is more irregular and porous indicating that the corrosion advanced through the carbides and it only marginally attacked the metal matrix. On the other hand, in **Error! Reference source not found.**

Fig. 9f, the front is more homogeneous and less porous, indicating that the corrosion was as fast through the matrix as through the carbides network.

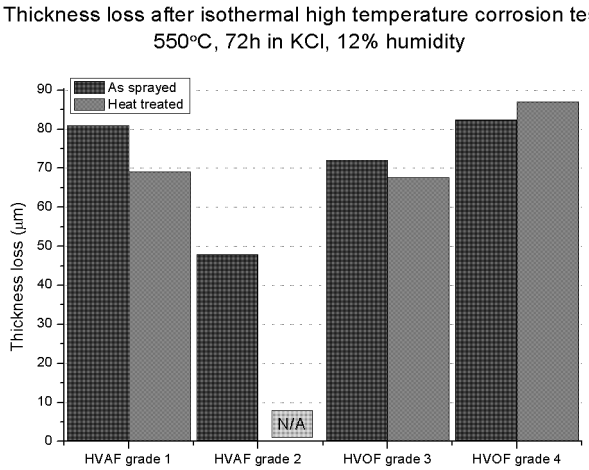

Fig. 9*: Comparison of the corrosion front of the coatings after 72 hours high temperature corrosion test at 550˚C under KCl and 12%humidty air. On the left column, the coatings HVAF grade 1, HVOF grade 3 and HVOF grade 4 were tested in as-sprayed condition(a, c, d respectively) while on the right column after heat treatment (b, d, f, respectively).*

4 Conclusions

In this study, the spray parameters of HVOF and HVAF processes were successfully designed in order to obtain four Cr_3C_2-NiCrMoNb coatings with tailored melting degree and carbon dissolution in the metal matrix. The initial stage of chlorine induced high temperature corrosion of HVAF and HVOF self-standing coatings was studied with thermogravimetric analyses.

The results showed that in the initial stage of the corrosion, the actual metal binder composition is probably the corrosion rate-controlling factor. On a second stage, the formation of a network of fine secondary carbides precipitates and their fast degradation is the rate-controlling factor. Based on these observations, the amount of carbon dissolution seems detrimental on the corrosion resistance of carbide-based coatings. Therefore, deposition by HVAF is recommended over HVOF for this composition due to its lower spray temperature and thus, reduced melting degree of the coating. Indeed, the sample HVAF-grade 2 largely outperformed the other tested coatings. However, a certain amount of melting degree and oxides content appear to be beneficial in order to reduce porosity and increase corrosion resistance.

4 Acknowledgments

The work has been done within the DIMECC HYBRIDS (Hybrid Materials) programme. We gratefully acknowledge the financial support from the Finnish Funding Agency for Innovation (Tekes) and the participating companies. A special thank goes also to Mr. Mikko Kylmälahti of Tampere University of Technology for spraying the HVOF and HVAF coatings, and Dr. Tech. Lucio Azzari and Dr. Tech. Matteo Maggioni for their support with the MatLab scripts.

References

1. P. Lempp, Biomass Co-Firing, *Technology brief E21–January. International Energy Agency-Energy Technology Systems Analysis Programme (IEA-ETSAP), and International Renewable Energy Agency (IRENA),* 2013,

2. J. Oh, M. McNallan, G. Lai, and M. Rothman, High Temperature Corrosion of Superalloys in an Environment Containing both Oxygen and Chlorine, *Metallurgical Transactions A,* 1986, **17**(6), 1087-1094.

3. M. Spiegel, A. Zahs, and H. Grabke, Fundamental Aspects of Chlorine Induced Corrosion in Power Plants, *Materials at high temperatures,* 2003, **20**(2), 153-159.

4. A. Zahs, M. Spiegel, and H.J. Grabke, Chloridation and Oxidation of Iron, Chromium, Nickel and their Alloys in Chloridizing and Oxidizing Atmospheres at 400–700 C, *Corros, Sci,* 2000, **42**(6), 1093-1122.

5. S. Cha and M. Spiegel, Local Reactions of KCl Particles with Iron, Nickel and Chromium Surfaces, *Materials and Corrosion,* 2006, **57**(2), 159-164.

8. B. Rukes and R. Taud, Status and Perspectives of Fossil Power Generation, *Energy,* 2004, **29**(12), 1853-1874.

9. P. Viklund, A. Hjörnhede, P. Henderson, A. Stålenheim, and R. Pettersson, Corrosion of Superheater Materials in a Waste-to-Energy Plant, *Fuel Process Technol,* 2013, **105**106-112.

10. A. Phongphiphat, C. Ryu, Y.B. Yang, K.N. Finney, A. Leyland, V.N. Sharifi, and J. Swithenbank, Investigation into High-Temperature Corrosion in a Large-Scale Municipal Waste-to-Energy Plant, *Corros, Sci,* 2010, **52**(12), 3861-3874.

11. M. Oksa, S. Tuurna, and T. Varis, Increased Lifetime for Biomass and Waste to Energy Power Plant Boilers with HVOF Coatings: High Temperature Corrosion Testing Under Chlorine-Containing Molten Salt, *J, Therm, Spray Technol,* 2013, **22**(5), 783-796.

12. M. Oksa, P. Auerkari, J. Salonen, and T. Varis, Nickel-Based HVOF Coatings Promoting High Temperature Corrosion Resistance of Biomass-Fired Power Plant Boilers, *Fuel Process Technol,* 2014, **125**236-245.

13. M. Oksa, Nickel-and Iron-Based HVOF Thermal Spray Coatings for High Temperature Corrosion Protection in Biomass-Fired Power Plant Boilers, 2015,

14. M. Uusitalo, P. Vuoristo, and T. Mäntylä, Elevated Temperature Erosion–corrosion of Thermal Sprayed Coatings in Chlorine Containing Environments, *Wear,* 2002, **252**(7), 586-594.

17. N. Otsuka, Effects of Fuel Impurities on the Fireside Corrosion of Boiler Tubes in Advanced Power Generating Systems—a Thermodynamic Calculation of Deposit Chemistry, *Corros, Sci,* 2002, **44**(2), 265-283.

18. U. Brill, J. Kloewer and D.C. Agarwal, *Influence of alloying elements on the chlorination behavior of nickel-and iron-based alloys,* 1996,

19. L. Nylöf and E. Häggblom, *Corrosion of experimental superheater alloys in waste fuel combustion,* 1997,

20. N. Otsuka, Chemistry and Melting Characteristics of Fireside Deposits Taken from Boiler Tubes in Waste Incinerators, *Corros, Sci,* 2011, **53**(6), 2269-2276.

21. Y. Kawahara, High Temperature Corrosion Mechanisms and Effect of Alloying Elements for Materials used in Waste Incineration Environment, *Corros, Sci,* 2002, **44**(2), 223-245.

23. W. Zhou, K. Zhou, C. Deng, K. Zeng, and Y. Li, Hot Corrosion Behaviour of HVOF-Sprayed Cr3C2-NiCrMoNbAl Coating, *Surface and Coatings Technology,* 2017, **309**849-859.

24. M. Uusitalo, R. Backman, L. Berger, P. Vuoristo, and T. Mäntylä, Oxidation Resistance of Carbides in Chlorine-Containing Atmospheres, *High Temp Mater Processes,* 2002, **21**(5), 307-320.

25. P. Vuoristo, Thermal Spray Coating Process, Comprehensive Materials Processing, 2014,

26. J. Guilemany, J. Nutting, and N. Llorcalsern, Microstructural Examination of HVOF Chromium Carbide Coatings for High-Temperature Applications, *J, Therm, Spray Technol,* 1996, **5**(4), 483-489.

27. S. Matthews, M. Hyland, and B. James, Long-Term Carbide Development in High-Velocity Oxygen Fuel/High-Velocity Air Fuel Cr3C2-NiCr Coatings Heat Treated at 900° C, *J, Therm, Spray Technol,* 2004, **13**(4), 526-536.

28. S. Matthews, B. James, and M. Hyland, High Temperature Erosion of Cr_3C_2-NiCr Thermal Spray coatings—The Role of Phase Microstructure, *Surface and Coatings Technology,* 2009, **203**(9), 1144-1153.

29. Y. Ding, T. Hussain, and D. McCartney, High-Temperature Oxidation of HVOF Thermally Sprayed Incur–Cr3C2 Coatings: Microstructure and Kinetics, *J, Mater, Sci,* 2015, **50**(20), 6808-6821.

30. International Organization for Standardization. ISO 17224: Corrosion of Metals and Alloys — Test Method for High Temperature Corrosion Testing of Metallic Materials by Application of a Deposit of Salt, Ash, Or Other Substances. First Edition 2015-04-15. ISO 17224:2015(E).

31. D. Fantozzi, V. Matikainen, M. Uusitalo, H. Koivuluoto, and P. Vuoristo, Chlorine-Induced High Temperature Corrosion of Inconel 625 Sprayed Coatings Deposited with Different Thermal Spray Techniques, *Surface and Coatings Technology,* 2017, **318**233-243.

32. NACE MR0175/ISO 15156-1, Petroleum and Natural Gas Industries-Materials for use in H2S Containing Environments in Oil and Gas Production-Part 1: General Principles for Selection of Cracking-Resistant Materials, 2001,

33. S. Matthews, M. Hyland, and B. James, Microhardness Variation in Relation to Carbide Development in Heat Treated Cr 3 C 2–NiCr Thermal Spray Coatings, *Acta Materialia,* 2003, **51**(14), 4267-4277.

34. S. Matthews, B. James, and M. Hyland, The Role of Microstructure in the High Temperature Oxidation Mechanism of Cr_3C_2–NiCr Composite Coatings, *Corros, Sci,* 2009, **51**(5), 1172-1180.

36. S. Matthews and L. Berger, Long-Term Compositional/Microstructural Development of Cr3C2-NiCr Coatings at 500 °C, 700 °C and 900 °C, *International Journal of Refractory Metals and Hard Materials,* 2016, **59**1-18.

37. V. Matikainen, G. Bolelli, H. Koivuluoto, M. Honkanen, M. Vippola, L. Lusvarghi, and P. Vuoristo, A Study of Cr3C2-Based HVOF-and HVAF-Sprayed Coatings: Microstructure and Carbide Retention, *J, Therm, Spray Technol,* 2017, **26**(6), 1239-1256.

38. K. Dobler, H. Kreye, and R. Schwetzke, Oxidation of Stainless Steel in the High Velocity Oxy-Fuel Process, *J, Therm, Spray Technol,* 2000, **9**(3), 407-413.

39. M. Hocking, V. Vasantasree, and P. Sidky, Metallic and Ceramic Coatings: Production, High-Temperature Properties, and Applications, 1988,

40. H. Nielsen, F. Frandsen, K. Dam-Johansen, and L. Baxter, The Implications of Chlorine-Associated Corrosion on the Operation of Biomass-Fired Boilers, *Progress in energy and combustion science,* 2000, **26**(3), 283-298.